

Edge-Corner Correspondence: Boundary-Obstructed Topological Phases with Chiral Symmetry

Motohiko Ezawa

Department of Applied Physics, University of Tokyo, Hongo 7-3-1, 113-8656, Japan

The bulk-edge correspondence characterizes topological insulators and superconductors. We generalize this concept to the bulk-corner correspondence and the edge-corner correspondence in two dimensions. In the *bulk-corner (edge-corner)* correspondence, the topological number is defined for the *bulk (edge)*, while the topological phase is evidenced by the emergence of zero-energy *corner* states. It is shown that the boundary-obstructed topological phases recently proposed are the edge-corner-correspondence type, while the higher-order topological phases are classified into the bulk-corner-correspondence type and the edge-corner-correspondence type. We construct a simple model exhibiting the edge-corner correspondence based on two Chern insulators having the *s*-wave, *d*-wave and s_{\pm} -wave pairings. It is possible to define topological numbers for the edge Hamiltonians, and we have zero-energy corner states in the topological phase. The emergence of zero-energy corner states is observable by measuring the impedance resonance in topological electric circuits.

Topological insulators and superconductors are one of the most studied fields in this decade¹⁻⁴. A topological number is defined for the bulk. The bulk gap must close at a topological phase transition point because the topological number cannot change its quantized value without gap closing. Consequently, the topological phase is evidenced by the emergence of gapless edge states although the bulk is gapped. This phenomenon is well known as the bulk-edge correspondence.

We generalize this concept to the bulk-corner correspondence and the edge-corner correspondence. For definiteness we consider two-dimensional systems, although generalization to higher dimensions is straightforward⁵. In the *bulk-corner (edge-corner)* correspondence, the topological number is defined for the *bulk (edge)*, while the topological phase is evidenced by the emergence of zero-energy *corner* states. There is a case where the topological number for the bulk is expressed in terms of two topological numbers for the two edges. It is proper to regard such a system to belong to the edge-corner-correspondence type. A typical example is given by systems having square lattice structure⁶.

Here we summarize the properties whether the gap is open or closed in the trivial and topological phases in the system subject to the bulk-edge, bulk-corner and edge-corner correspondences as follows:

		trivial	PTP	topological	
bulk-edge:	bulk	o	×	o	, (1)
	edge	o	×	×	

		trivial	PTP	topological	
bulk-corner:	bulk	o	×	o	, (2)
	edge	o	×	o	
	corner	o	×	×	

		trivial	PTP	topological	
edge-corner:	bulk	o	o	o	, (3)
	edge	o	×	o	
	corner	o	×	×	

where o and × indicate that the gap is open and closed; PTP stands for the phase-transition point.

It is important to reexamine higher-order topological

insulators⁶⁻¹⁹ and superconductors^{8,20-22} according to this classification. Clearly they are classified into these two types: A typical example of the edge-corner-correspondence type is given by the quadrupole insulator^{6,12}, while a typical example of the bulk-corner-correspondence type is given by the Kagome lattice¹⁵.

The notion of boundary-obstructed topological phases was recently introduced²³. Several works on them have successfully been reported²⁴⁻²⁶. It has been proposed that they are realized in ion-based topological superconductors²⁷. These phases are characterized by the property that the bulk-band gap does not close but the edge-gap closes at the topological phase transition point. Referring to the properties listed in Eqs.(2) and (3), they must belong to the edge-corner-correspondence type.

In this paper, we construct a simple model realizing the edge-corner correspondence and the boundary-obstructed topological phase in order to make a clear understanding of these phenomena. The model consists of two Chern insulators with the opposite Chern numbers. We introduce pairing interactions including the *s*-wave, *d*-wave and s_{\pm} -wave pairing. The system has chiral symmetry. The topological class is BDI, which allows a topological phase in one dimension but none in two dimensions²⁸. Accordingly, a topological phase transition may occur, where the edge gap is closed while the band gap is open, and zero-energy corner states emerge in the topological phase. It is possible to define the topological numbers Γ_x and Γ_y for the edge Hamiltonians along the *x* and *y* axes, and the topological number $\Gamma_x\Gamma_y$ for the bulk. We point out that the edge-corner correspondence is observable by the impedance measurement in electric circuits.

Model Hamiltonian: We start with the Chern insulator on square lattice, whose Hamiltonian is given by

$$H_{\text{Chern}} = M\sigma_z + \lambda_x\sigma_x \sin k_x + \lambda_y\sigma_y \sin k_y, \quad (4)$$

with Pauli matrices σ_i , spin-orbit interactions λ_x and λ_y , and

$$M = t_x \cos k_x + t_y \cos k_y - \mu, \quad (5)$$

where t_x and t_y are hopping parameters, and μ is the chemical potential.

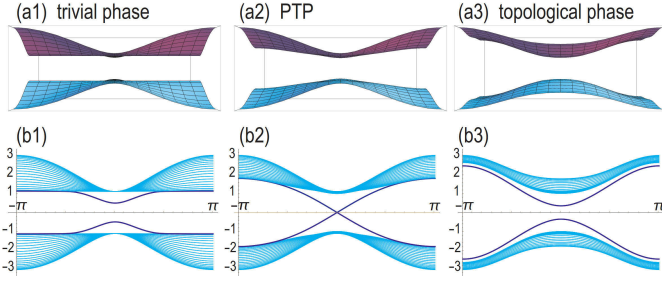


FIG. 1: Band structures of (a) the bulk and (b) a nanoribbon. The nanoribbon bands consist of the bulk bands (in cyan) and the edge bands (in blue). The edge becomes gapless only at the topological phase transition point as in (b2), while the bulk gap is always open. We have used parameters $\Delta_d = 0$ for (a1) and (b1), $\Delta_d = 0.5t$ for (a2) and (b2), and $\Delta_d = t$ for (a3) and (b3). We have set $t_x = t_y = \lambda_x = \lambda_y = \mu = t$, $\Delta_0 = 0.5t$ and $\Delta_{s\pm} = 0$. The nanoribbon width is $W = 20$.

We propose to construct a chiral symmetric model as

$$H = \tau_z H_{\text{Chern}} + \tau_x H_{\Delta}, \quad (6)$$

where we assume a pairing Hamiltonian²⁰ in the form of

$$H_{\Delta} = \Delta_0 + \Delta_x \cos k_x + \Delta_y \cos k_y, \quad (7)$$

with

$$\Delta_x = \Delta_{s\pm} + \Delta_d, \quad \Delta_y = \Delta_{s\pm} - \Delta_d. \quad (8)$$

Here, Δ_0 , Δ_d and $\Delta_{s\pm}$ are the gap parameters due to the s -wave, d -wave and s_{\pm} -wave pairings^{29,30}, respectively.

Symmetries: The Hamiltonian H has chiral symmetry, $\{H, \tau_y\} = 0$. The system has time-reversal symmetry, $TH(k)T^{\dagger} = H(-k)$ with $T = \sigma_x \tau_x K$, where K takes complex conjugation. The system has particle-hole symmetry, $\Xi H(k)\Xi^{\dagger} = -H(-k)$ with $\Xi = \sigma_x \tau_z K$. Hence, the system belongs to the class BDI, where there is no topological phase in two dimensions²⁸. In addition, the system has parity symmetry $PH(k)P^{\dagger} = H(-k)$ with $P = \sigma_z$.

Bulk: The energy spectrum of H is given by

$$E = \pm \sqrt{E_{\text{Chern}}^2 + E_{\Delta}^2}, \quad (9)$$

where

$$E_{\text{Chern}} = \sqrt{M^2 + \lambda_x^2 \sin^2 k_x + \lambda_y^2 \sin^2 k_y} \quad (10)$$

is the energy of H_{Chern} , and

$$E_{\Delta} = \Delta_0 + \Delta_x \cos k_x + \Delta_y \cos k_y \quad (11)$$

is the energy of H_{Δ} . The bulk-band gap is

$$2E(0,0) = 2\sqrt{(t_x + t_y - \mu)^2 + \Delta_0^2}. \quad (12)$$

The bulk gap E never closes when the E_{Chern} is gapped.

We show the band structure for various Δ_d in Fig.1(a1)~(a3) by setting $t_x = t_y = \lambda_x = \lambda_y = \mu = t$,

$\Delta_0 = 0.5t$ and $\Delta_{s\pm} = 0$ for simplicity. The bulk gap is independent of the magnitude of Δ_d .

Edge theory: We show the band structure of a nanoribbon for various Δ_d in Fig.1(b1)~(b3). The edge states become gapless at a certain phase-transition point as in Fig.1(b2). In order to determine this point and to construct the topological phase diagram, we derive the edge Hamiltonians along the x and y axes.

We first construct the edge Hamiltonian along the y axis. We make a Taylor expansion at the Γ point and decompose the Hamiltonian (6) into the unperturbed Hamiltonian H_0 and the perturbed Hamiltonian H_1 , $H = H_0 + H_1$, with

$$H_0 = \tau_z [\sigma_z (2^{-1} t_x \partial_x^2 + t_x + t_y - \mu) - i \lambda_x \sigma_x \partial_x], \quad (13)$$

$$H_1 = \lambda_y k_y \tau_z \sigma_y + (\Delta_0 + \Delta_x + \Delta_y) \tau_x + 2^{-1} \Delta_x \tau_x \partial_x^2, \quad (14)$$

where we have omitted insignificant k_y^2 terms²⁰. Setting $H_0 = \tau_z H'_0$, we solve the eigen equation of H'_0 as $\psi = (\psi_1, i\eta\psi_1)$ with $\psi_1 = e^{-\kappa x} e^{ik_y y}$, where the penetration depth is

$$\kappa = \left(\eta \lambda_x \pm \sqrt{\lambda_x^2 + 2t_x m} \right) / t_x, \quad (15)$$

with $m = \mu - t_x - t_y$. By taking an expectation value of H_1 by ψ , we obtain the edge Hamiltonian along the y axis as

$$H_y = \eta_y \lambda_y k_y \tau_z + \bar{\Delta}_y \tau_x, \quad (16)$$

with

$$\bar{\Delta}_\alpha = \Delta_0 + \Delta_\alpha m / t_\alpha, \quad (17)$$

where $\alpha = x, y$; $\eta_x = 1$ for the lower and $\eta_x = -1$ for upper edges. The edge gap closes at $\bar{\Delta}_x = 0$.

Similarly we obtain the edge Hamiltonian for the x axis as

$$H_x = \eta_x \lambda_x k_x \tau_z + \bar{\Delta}_x \tau_x, \quad (18)$$

where $\eta_y = 1$ for the right and $\eta_y = -1$ for left edges. The edge gap closes at $\bar{\Delta}_y = 0$.

Edge symmetries: The edge Hamiltonian H_α has chiral symmetry, $\{H_\alpha, \tau_y\} = 0$. The system has time-reversal symmetry, $TH(k)T^{\dagger} = H(-k)$ with $T = \tau_x K$, where K takes complex conjugation. The system has particle-hole symmetry, $\Xi H(k)\Xi^{\dagger} = -H(-k)$ with $\Xi = \tau_z K$. Hence, the system belongs to the class BDI, where there is a topological phase in one dimensions²⁸. In addition, the system has parity symmetry $PH(k)P^{\dagger} = H(-k)$ with $P = \tau_x$.

Edge topological numbers: The edge chiral index is defined by

$$\Gamma_\alpha = \frac{1}{2\pi i} \text{Tr} \int \tau_y H_\alpha^{-1} \partial_\alpha H_\alpha dk_\alpha \quad (19)$$

with $\alpha = x, y$, which is a symmetry-protected-topological number associated with the chiral symmetry. With the aid of the relation

$$H_\alpha^{-1} \partial_\alpha H_\alpha = \frac{-2i \bar{\Delta}_\alpha}{\lambda_\alpha^2 k_\alpha^2 + \bar{\Delta}_\alpha^2}, \quad (20)$$

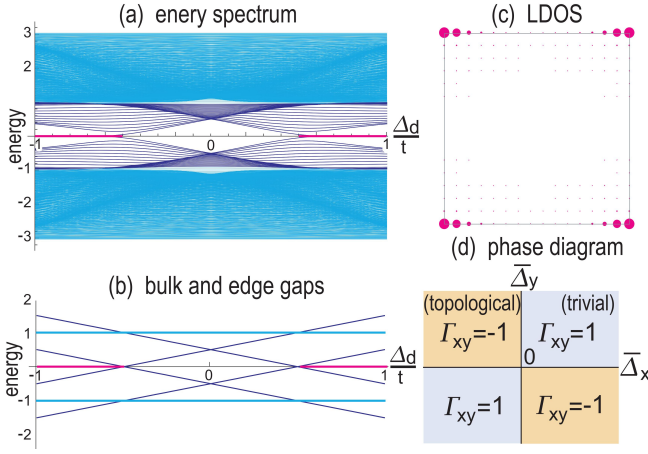


FIG. 2: (a) Energy spectrum in square geometry. The bulk and edge bands are shown in cyan and blue, respectively. The bulk gap is open at the topological phase transition point. The horizontal axis is Δ_d/t , while the vertical axis is the energy in unit of t . We have used a square with size $N = 32$. (b) Bulk gap (in cyan) and edge gap (in blue) as a function of Δ_d/t , which are obtained analytically. The horizontal lines (in magenta) represent zero-energy corner states. (c) LDOS for zero-energy corner states. All other parameters are the same as in Fig.1. (d) Topological phase diagram is determined by the sign of $\bar{\Delta}_x \bar{\Delta}_y$. We can assign the topological number Γ_{xy} to this phase diagram, where $\Gamma_{xy} = 1$ ($\Gamma_{xy} = -1$) stands for the trivial (topological) phase.

it is calculated as

$$\Gamma_\alpha = -\eta_\alpha \text{sgn} [\lambda_\alpha \bar{\Delta}_\alpha]. \quad (21)$$

We can differentiate the trivial and topological phases by the conditions $\bar{\Delta}_\alpha > 0$ and $\bar{\Delta}_\alpha < 0$, respectively.

Corner theory: We calculate numerically the energy spectrum and show it as a function of Δ_d for square geometry in Fig.2(a). It consists of the bulk and edge states shown in blue and cyan, respectively. On the other hand, we can derive analytically the bulk-band gap as in Eq.(12) and the edge-band gap as in Eq.(17), which we show in Fig.2(b). The numerical and analytical results agree very well. Additionally, we have shown zero-energy corner states in magenta in Figs.2(a) and (b), which we derive analytically in what follows. It is prominent that the edge gap closes only at the phase transition point ($\bar{\Delta}_\alpha = 0$). We show the local density of states (LDOS) for the zero-energy corner states in Fig.2(c).

We study the corner states analytically. They are described by the Jackiw-Rebbi solutions³¹ of the edge Hamiltonians. The zero-energy solution along the x -axis is derived by solving (18), or

$$H_x = -i\eta_x \lambda_x \tau_z \partial_x + \bar{\Delta}_x \tau_x. \quad (22)$$

The solution is obtained as $\psi_x = (\psi_{x1}, i\eta_x \psi_{x1})$ with

$$\psi_x(x) = \exp[\pm(\eta_x/\lambda_x)\bar{\Delta}_x x]. \quad (23)$$

Similarly, the zero-energy solution along the y -axis reads

$$\psi_y(y) = \exp[\mp(\eta_y/\lambda_y)\bar{\Delta}_y y]. \quad (24)$$

The wave functions are well defined when they converge, leading to the condition,

$$\bar{\Delta}_x \bar{\Delta}_y < 0. \quad (25)$$

The zero-energy corner states emerge only in this case.

Topological phase diagram: We construct the topological phase diagram in the $(\bar{\Delta}_x, \bar{\Delta}_y)$ plane. As we have just derived, the condition for the emergence of the zero-energy corner states is given by (25), or $\bar{\Delta}_x \bar{\Delta}_y < 0$, where the system is topological. On the other hand, the system is trivial for $\bar{\Delta}_x \bar{\Delta}_y > 0$, because there are no zero-energy states. The topological phase diagram is determined by these conditions as in Fig.2(d), with the phase boundary being given by $\bar{\Delta}_x \bar{\Delta}_y = 0$.

We may define the topological number for the bulk, which reproduces the phase diagram determined in terms of $\bar{\Delta}_x \bar{\Delta}_y$. With the use of Γ_α defined by (21), it is given by

$$\Gamma_{xy} = \Gamma_x \Gamma_y, \quad (26)$$

where $\Gamma_{xy} = 1$ for the trivial phase and $\Gamma_{xy} = -1$ for the topological phase as in Fig.2(d).

Electric-circuit realization: Electric circuits provide us with an ideal playground to realize various topological phases³²⁻⁴². Especially, higher-order topological phases^{32,38,43,44} are simulated based on electric circuits. Topological corner states are observed by impedance resonance³².

Electric-circuit realization is based on the correspondence^{32,33} between the Hamiltonian H and the circuit Laplacian J such that $J = i\omega H$. The Hamiltonian H_{chem} is already discussed in electric circuits⁴¹. The circuit corresponding to Hamiltonian H can be constructed in a similar manner. The capacitance contribute to $i\omega C$, while the inductance contributes to $1/i\omega L$ in the circuit Laplacian. It corresponds to the positive and negative hoppings in the Hamiltonian. The imaginary hoppings are represented by the operational amplifiers⁴⁰. We tune the frequency ω to be the critical frequency $\omega_0 = 1/\sqrt{LC}$ so that the circuit Laplacian is identical to the Hamiltonian.

Admittance is obtained by the eigenvalue of the circuit Laplacian³⁴, which corresponds to the eigen energy of the Hamiltonian. We show the admittance spectrum as a function of ω in Fig.3(a). The zero-admittance state appears in the topological phase, while it is absent in the trivial phase.

The circuit Laplacian is explicitly given by

$$J = \begin{pmatrix} f_1 & g_1 & h & 0 \\ g_2 & f_2 & 0 & h \\ h & 0 & f_2 & g_2 \\ 0 & h & g_1 & f_1 \end{pmatrix} \quad (27)$$

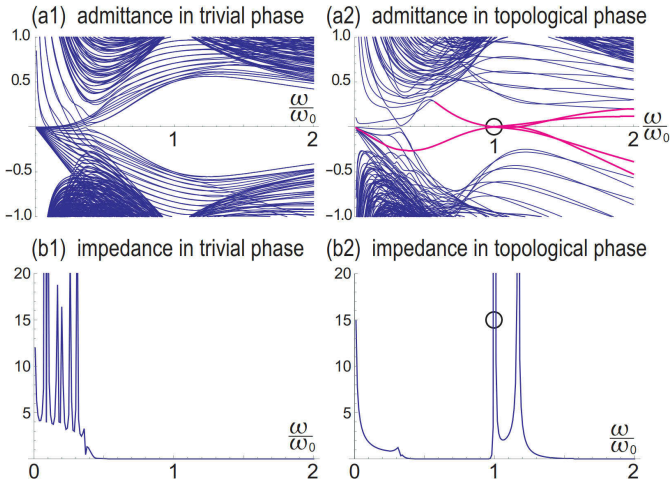


FIG. 3: (a) Admittance spectrum in square geometry (a1) for the trivial phase and (a2) for the topological phase. The horizontal axis is ω/ω_0 . There are four-fold degenerate zero-admittance states at $\omega_0 = \omega$ in the topological phase. They are marked by a black circle in (a2). (b) Impedance as a function of ω (b1) in the trivial phase and (b2) in the topological phase. There is a strong peak at $\omega = \omega_0$ in the topological phase, as marked by a black circle in (a2). The horizontal axis is ω/ω_0 . We have used a square with size $N = 16$.

with

$$\begin{aligned}
 f_1 &= i\omega (C_x \cos k_x + C_y \cos k_y) - i\omega C_x - i\omega C_y + i\omega C_m, \\
 f_2 &= (i\omega L_x)^{-1} \cos k_x + (i\omega L_y)^{-1} \cos k_y \\
 &\quad - (i\omega L_x)^{-1} - (i\omega L_y)^{-1} + (i\omega L_m)^{-1}, \\
 g_1 &= i\omega C_X e^{ik_y} + (i\omega L_X)^{-1} e^{-ik_y} + R^{-1} (e^{ik_x} - e^{-ik_x}), \\
 g_2 &= (i\omega L_X)^{-1} e^{ik_y} + i\omega C_X e^{-ik_y} + R^{-1} (e^{ik_x} - e^{-ik_x}), \\
 h &= i\omega C_{\Delta 0} + i\omega C_{\Delta x} \cos k_x + i\omega C_{\Delta y} \cos k_y. \quad (28)
 \end{aligned}$$

It is straightforward to design electric circuits corresponding to this circuit Laplacian.

We analyze the impedance³⁴, which is defined by $Z_{ab} = V_a/I_b = G_{ab}$ where $G = J^{-1}$ is the Green function. It diverges at the frequency where the admittance is zero ($J = 0$). Note that the impedance and the admittance have inverse relation. Taking the nodes a and b at two corners, we show the impedance in the trivial and topological phases in Figs.3(b1) and (b2), respectively. A strong impedance peak is observed at the critical frequency ω_0 in the topological phase, while it is absent in the trivial phase. It signals the emergence of zero-energy corner states. Hence, the edge-corner correspondence is observable in electric circuits.

Discussions: We have presented a classification of various higher-order topological phases based on the bulk-corner and edge-corner correspondences. We have constructed a simple model exhibiting the edge-corner correspondence, where topological numbers are defined for edges. It provides us with a clear picture of the boundary-obstructed topological phase transition. Furthermore, we have argued that the emergence of topological corner states is detectable by observing impedance peaks in topological electric circuit. The merit of electric circuits is that we can tune the values of elements relatively easily, which enables to realize a topological phase transition.

The generalization to three dimensions is straight forward. We may consider bulk-hinge, surface-hinge correspondences for the second-order topological phases⁵. We may also consider bulk-corner, surface-corner and hinge-corner correspondences for the third-order topological phases⁵.

The author is very much grateful to N. Nagaosa for helpful discussions on the subject. This work is supported by the Grants-in-Aid for Scientific Research from MEXT KAKENHI (Grants No. JP17K05490 and No. JP18H03676). This work is also supported by CREST, JST (JPMJCR16F1).

-
- ¹ M. Z. Hasan and C. L. Kane, Rev. Mod. Phys. **82**, 3045 (2010).
² X.-L. Qi and S.-C. Zhang, Rev. Mod. Phys. **83**, 1057 (2011).
³ M. Leijnse and K. Flensberg, Semicond. Sci. Technol. **27**, 124003 (2012).
⁴ C. W. J. Beenakker, Annu. Rev. Con. Mat. Phys. **4**, 113 (2013).
⁵ See Supplementary Material for the generalization of the bulk-boundary correspondence to include the second-order topological phases and the third-order topological phases in three dimensions.
⁶ W. A. Benalcazar, B. A. Bernevig, and T. L. Hughes, **357**, 61 (2017).
⁷ F. Zhang, C.L. Kane and E.J. Mele, Phys. Rev. Lett. **110**, 046404 (2013).
⁸ F. Schindler, A. Cook, M. G. Vergniory, and T. Neupert, in APS March Meeting (2017).
⁹ Y. Peng, Y. Bao, and F. von Oppen, Phys. Rev. B **95**, 235143 (2017).
¹⁰ J. Langbehn, Y. Peng, L. Trifunovic, F. von Oppen, and P. W. Brouwer, Phys. Rev. Lett. **119**, 246401 (2017).
¹¹ Z. Song, Z. Fang, and C. Fang, Phys. Rev. Lett. **119**, 246402 (2017).
¹² W. A. Benalcazar, B. A. Bernevig, and T. L. Hughes, Phys. Rev. B **96**, 245115 (2017).
¹³ F. Schindler, A. M. Cook, M. G. Vergniory, Z. Wang, S. S. P. Parkin, B. A. Bernevig, and T. Neupert, Science Advances 01 Jun 2018: Vol. 4, no. 6, eaat0346.
¹⁴ C. Fang, L. Fu, Science Advances **5**, eaat2374 (2019).
¹⁵ M. Ezawa, Phys. Rev. Lett. **120**, 026801 (2018).
¹⁶ M. Ezawa, Phys. Rev. B **98**, 045125 (2018).
¹⁷ M. Geier, L. Trifunovic, M. Hoskam, and P. W. Brouwer, Phys. Rev. B **97**, 205135 (2018).
¹⁸ M. Ezawa, Phys. Rev. B **97**, 155305 (2018).
¹⁹ E. Khalaf, Phys. Rev. B **97**, 205136 (2018).
²⁰ Z. Yan, F. Song and Z. Wang, Phys. Rev. Lett. **121**, 096803 (2018).
²¹ Q. Wang, C.-C. Liu, Y.-M. Lu and F. Zhang, Phys. Rev. Lett. **121**, 186801 (2018).
²² Y. Wang, M. Lin, T. L. Hughes, Phys. Rev. B **98**, 165144 (2018).
²³ E. Khalaf, W. A. Benalcazar, T. L. Hughes and R. Queiroz, arXiv:1908.00011
²⁴ K. Asaga and T. Fukui, arXiv:2002.04209
²⁵ J. Claes and T. L. Hughes, arXiv:2005.09659

- ²⁶ A. Tiwari, A. Jahin and Y. Wang, arXiv:2005.12291
- ²⁷ X. Wu, W. A. Benalcazar, Y. Li, R. Thomale, C.-X. Liu, and J. Hu, arXiv:2003.12204
- ²⁸ A. P. Schnyder, Shinsei Ryu, A. Furusaki and A. W. W. Ludwig, Phys. Rev. B **78** 195125 (2008).
- ²⁹ G. R. Stewart, Reviews of Modern Physics 83, 1589 (2011)
- ³⁰ P. J. Hirschfeld, M. M. Korshunov and I. I. Mazin, Reports on Progress in Physics 74, 124508 (2011)
- ³¹ R. Jackiw and C. Rebbi, Phys. Rev. D 13 3398 (1976)
- ³² S. Imhof, C. Berger, F. Bayer, J. Brehm, L. Molenkamp, T. Kiessling, F. Schindler, C. H. Lee, M. Greiter, T. Neupert, R. Thomale, Nat. Phys. **14**, 925 (2018).
- ³³ C. H. Lee, S. Imhof, C. Berger, F. Bayer, J. Brehm, L. W. Molenkamp, T. Kiessling and R. Thomale, Communications Physics, **1**, 39 (2018).
- ³⁴ T. Helbig, T. Hofmann, C. H. Lee, R. Thomale, S. Imhof, L. W. Molenkamp and T. Kiessling, Phys. Rev. B 99, 161114 (2019).
- ³⁵ Y. Lu, N. Jia, L. Su, C. Owens, G. Juzeliunas, D. I. Schuster and J. Simon, Phys. Rev. B **99**, 020302 (2019).
- ³⁶ K. Luo, R. Yu and H. Weng, Research (2018), ID 6793752.
- ³⁷ E. Zhao, Ann. Phys. **399**, 289 (2018).
- ³⁸ M. Ezawa, Phys. Rev. B **98**, 201402(R) (2018).
- ³⁹ M. Serra-Garcia, R. Susstrunk and S. D. Huber, Phys. Rev. B **99**, 020304 (2019).
- ⁴⁰ T. Hofmann, T. Helbig, C. H. Lee, M. Greiter, R. Thomale, Phys. Rev. Lett. **122**, 247702 (2019).
- ⁴¹ M. Ezawa, Phys. Rev. B 100, 045407 (2019)
- ⁴² M. Ezawa, cond-mat/arXiv:1907.06911
- ⁴³ M. Ezawa, Phys. Rev. B **99**, 201411(R) (2019).
- ⁴⁴ M. Ezawa, Phys. Rev. B **99**, 121411(R) (2019).

Supplemental Material

Edge-Corner Correspondence: Boundary-Obstructed Topological Phases with Chiral Symmetry

Motohiko Ezawa

Department of Applied Physics, University of Tokyo, Hongo 7-3-1, 113-8656, Japan

S1. Second-order topological phases in three dimensions

The second-order topological phases in three dimensions are characterized by the phenomena that gapless hinge states emerge although the bulk and the surface are gapped. They are classified into the bulk-hinge-correspondence type and the surface-hinge-correspondence type according to the geometrical object upon which the topological numbers are defined. Hereafter, let us abbreviate the A-B-correspondence type as the A-B type. (i) In the bulk-hinge type, the bulk gap closes at the phase transition point. The topological number is defined for the bulk. (ii) In the surface-hinge type, the surface gap closes but the bulk gap remains to open at the phase transition point. The topological number is defined for the surface.

These phenomena are summarized as

$$\begin{array}{l}
 \text{(i) bulk-hinge correspondence:} \\
 \begin{array}{l}
 \text{bulk} \\
 \text{surface} \\
 \text{hinge}
 \end{array}
 \begin{array}{ccc}
 \text{trivial} & \text{PTP} & \text{topological} \\
 \circ & \times & \circ \\
 \circ & \times & \circ \\
 \circ & \times & \circ
 \end{array}
 \end{array}
 , \tag{S1}$$

$$\begin{array}{l}
 \text{(ii) surface-hinge correspondence:} \\
 \begin{array}{l}
 \text{bulk} \\
 \text{surface} \\
 \text{hinge}
 \end{array}
 \begin{array}{ccc}
 \text{trivial} & \text{PTP} & \text{topological} \\
 \circ & \circ & \circ \\
 \circ & \times & \circ \\
 \circ & \times & \circ
 \end{array}
 \end{array}
 . \tag{S2}$$

S2. Third-order topological phases in three dimensions

The third-order topological phases in three dimensions are characterized by the phenomena that zero-energy corner states emerge although the bulk, the surface and the hinge are gapped. They are classified into three types, the bulk-corner type, surface-corner type and the hinge-corner type, according to the geometrical object upon which the topological numbers are defined. (i) In the bulk-corner type, the bulk gap closes at the phase transition point. The topological number is defined for the bulk. (ii) In the surface-corner type, the surface gap closes but the bulk gap remains to open at the phase transition point. The topological number is defined for the surface. (iii) In the hinge-corner type, the hinge gap closes but the bulk and surface gaps remain to open at the phase transition point. The topological number is defined for the hinge.

These phenomena are summarized as

$$\begin{array}{l}
 \text{(i) bulk-corner correspondence:} \\
 \begin{array}{l}
 \text{bulk} \\
 \text{surface} \\
 \text{hinge} \\
 \text{corner}
 \end{array}
 \begin{array}{ccc}
 \text{trivial} & \text{PTP} & \text{topological} \\
 \circ & \times & \circ \\
 \circ & \times & \circ \\
 \circ & \times & \circ \\
 \circ & \times & \times
 \end{array}
 \end{array}
 , \tag{S3}$$

$$\begin{array}{l}
 \text{(ii) surface-corner correspondence:} \\
 \begin{array}{l}
 \text{bulk} \\
 \text{surface} \\
 \text{hinge} \\
 \text{corner}
 \end{array}
 \begin{array}{ccc}
 \text{trivial} & \text{PTP} & \text{topological} \\
 \circ & \circ & \circ \\
 \circ & \times & \circ \\
 \circ & \times & \circ \\
 \circ & \times & \times
 \end{array}
 \end{array}
 , \tag{S4}$$

$$\begin{array}{l}
 \text{(iii) hinge-corner correspondence:} \\
 \begin{array}{l}
 \text{bulk} \\
 \text{surface} \\
 \text{hinge} \\
 \text{corner}
 \end{array}
 \begin{array}{ccc}
 \text{trivial} & \text{PTP} & \text{topological} \\
 \circ & \circ & \circ \\
 \circ & \circ & \circ \\
 \circ & \times & \circ \\
 \circ & \times & \times
 \end{array}
 \end{array}
 . \tag{S5}$$